

Detection statistics of the RadioAstron AGN survey

Y. Y. Kovalev^{a,b,c}, N. S. Kardashev^{1a}, K. V. Sokolovsky^{a,d,e}, P. A. Voitsik^a,
 T. An^f, J. M. Anderson^{g,h}, A. S. Andrianov^a, V. Yu. Avdeev^a, N. Bartelⁱ,
 H. E. Bignall^j, M. S. Burgin^a, P. G. Edwards^k, S. P. Ellingsen^l, S. Frey^m,
 C. García-Miróⁿ, M. P. Gawroński^o, F. D. Ghigo^p, T. Ghosh^{p,q},
 G. Giovannini^{r,s}, I. A. Girin^a, M. Giroletti^r, L. I. Gurvits^{t,u},
 D. L. Jauncey^{k,v}, S. Horiuchi^w, D. V. Ivanov^x, M. A. Kharinov^x,
 J. Y. Koay^y, V. I. Kostenko^a, A. V. Kovalenko^{aa}, Yu. A. Kovalev^a,
 E. V. Kravchenko^{r,a}, M. Kunert-Bajraszewska^o, A. M. Kutkin^{a,z},
 S. F. Likhachev^a, M. M. Lisakov^{c,a}, I. D. Litovchenko^a, J. N. McCallum^l,
 A. Melis^{ab}, A. E. Melnikov^x, C. Migoni^{ab}, D. G. Nair^t, I. N. Pashchenko^a,
 C. J. Phillips^k, A. Polatidis^z, A. B. Pushkarev^{a,ad}, J. F. H. Quick^{ae},
 I. A. Rakhimov^x, C. Reynolds^j, J. R. Rizzo^{af}, A. G. Rudnitskiy^a,
 T. Savolainen^{ag,ah,c}, N. N. Shakhvorostova^a, M. V. Shatskaya^a,
 Z.-Q. Shen^{f,ac}, M. A. Shchurov^a, R. C. Vermeulen^z, P. de Vicente^{ai},
 P. Wolak^o, J. A. Zensus^c, V. A. Zuga^a

^a*Astro Space Center of Lebedev Physical Institute, Profsoyuznaya St. 84/32,
 117997 Moscow, Russia*

^b*Moscow Institute of Physics and Technology, Dolgoprudny, Institutskiy per., 9, Moscow
 region, 141700, Russia*

^c*Max-Planck-Institut für Radioastronomie, Auf dem Hügel 69, 53121 Bonn, Germany*

^d*Department of Physics and Astronomy, Michigan State University, East Lansing,
 Michigan 48824, USA*

^e*Sternberg Astronomical Institute, Moscow State University, Universitetskii pr. 13,
 119992 Moscow, Russia*

^f*Shanghai Astronomical Observatory, Chinese Academy of Sciences, Shanghai 200030,
 Peoples Republic of China*

^g*Institute of Geodesy and Geoinformation Science, Technical University of Berlin, Strae
 des 17. Juni 135, 10623 Berlin, Germany*

^h*Department of Geodesy, GFZ German Research Centre for Geosciences, Telegrafenberg,
 14473 Potsdam, Germany*

ⁱ*York University, 4700 Keele Street, Toronto, ON, M3J 1P3, Canada*

^j*CSIRO Astronomy and Space Science, PO Box 1130, Bentley WA 6102, Australia*

^k*CSIRO Astronomy and Space Science, PO Box 76, Epping, NSW 1710, Australia*

^l*School of Natural Sciences, Private Bag 37, University of Tasmania, Hobart 7001, TAS,
 Australia*

¹Deceased

- ^m*Konkoly Observatory, MTA Research Centre for Astronomy and Earth Sciences,
Konkoly Thege M. út 15-17, 1121 Budapest, Hungary*
- ⁿ*Square Kilometre Array Organisation (SKAO), Jodrell Bank Observatory, Lower
Withington, Macclesfield, Cheshire SK11 9DL, United Kingdom*
- ^o*Centre for Astronomy, Faculty of Physics, Astronomy and Informatics, NCU,
Grudziacka 5, 87-100 Toruń, Poland*
- ^p*Green Bank Observatory, P.O. Box 2, Green Bank, WV 24944, USA*
- ^q*Arecibo Observatory, HC03 Box 53995, Arecibo PR 00612*
- ^r*INAF Istituto di Radioastronomia, via Gobetti 101, I-40129 Bologna, Italy*
- ^s*Dipartimento di Fisica e Astronomia, Università di Bologna, via Gobetti 93/2 40129
Bologna, Italy*
- ^t*Joint Institute for VLBI ERIC, Oude Hoogeveensedijk 4, 7991 PD, Dwingeloo, The
Netherlands*
- ^u*Department of Astrodynamics and Space Missions, Delft University of Technology,
Kluyverweg 1, 2629 HS Delft, The Netherlands*
- ^v*Research School of Astronomy & Astrophysics, Australian National University,
Canberra ACT, Australia*
- ^w*CSIRO Astronomy and Space Science, Canberra Deep Space Communication Complex
PO Box 1035, Tuggeranong, ACT 2901, Australia*
- ^x*Institute of Applied Astronomy, Russian Academy of Sciences, nab. Kutuzova 10,
191187 St. Petersburg, Russia*
- ^y*Institute of Astronomy and Astrophysics, Academia Sinica, PO Box 23-141, Taipei
10617, Taiwan*
- ^z*ASTRON, Netherlands Institute for Radio Astronomy, Oude Hoogeveensedijk 4,
7991 PD Dwingeloo, the Netherlands*
- ^{aa}*Pushchino Radio Astronomy Observatory of Astro Space Center of Lebedev Physical
Institute, Moscow region, 142290 Pushchino, Russia*
- ^{ab}*Cagliari Astronomical Observatory of National Institute for Astrophysics, Viale della
scienza 5, 09047 Selargius, Italy*
- ^{ac}*Key Laboratory of Radio Astronomy, Chinese Academy of Sciences, Nanjing 210008,
Peoples Republic of China*
- ^{ad}*Crimean Astrophysical Observatory, Nauchny 298409, Russia*
- ^{ae}*Hartebeesthoek Radio Astronomy Observatory, Box 443, Krugersdorp 1740, South
Africa*
- ^{af}*Centro de Astrobiología (INTA-CSIC), Ctra. M-108, km. 4, E-28850 Torrejón de
Ardoz, Madrid, Spain*
- ^{ag}*Aalto University Department of Electronics and Nanoengineering, PL 15500, FI-00076
Aalto, Finland*
- ^{ah}*Aalto University Metsähovi Radio Observatory, Metsähovintie 114, 02540 Kylmälä,
Finland*
- ^{ai}*Observatorio de Yebes (IGN), Cerro de la Palera SN, 19141, Yebes, Guadalajara, Spain*

Abstract

The largest Key Science Program of the *RadioAstron* space VLBI mission is a survey of active galactic nuclei (AGN). The main goal of the survey is to measure and study the brightness of AGN cores in order to better understand the physics of their emission while taking interstellar scattering into consideration. In this paper we present detection statistics for observations on ground-space baselines of a complete sample of radio-strong AGN at the wavelengths of 18, 6, and 1.3 cm. Two-thirds of them are indeed detected by *RadioAstron* and are found to contain extremely compact, tens to hundreds of μas structures within their cores.

Keywords: active galactic nuclei, quasars, galaxies: jets, radio continuum: galaxies, space VLBI

1. Probing the emission mechanism of AGN jets

The current paradigm for AGN assumes that their radio emission is synchrotron in nature and is produced by relativistic electrons. In this model, the intrinsic brightness temperatures cannot exceed $10^{11.5}$ K (Kellermann and Pauliny-Toth, 1969; Readhead, 1994). According to calculations by Readhead (1994), it takes about a day for inverse Compton cooling (the so-called “Compton Catastrophe”) to lower brightness temperatures initially exceeding such a limit due to, e.g., non-stationary injection of very high energy electrons in AGN cores, to values below this limit. However, the observed AGN emission might appear brighter due to Doppler boosting through bulk motion of the emitting plasma (e.g., Shklovskii, 1964). Very long baseline interferometry (VLBI) kinematic studies of AGN show no evidence for Lorentz factors larger than 50 (Cohen et al., 2007), so Doppler boosting cannot increase the apparent jet brightness by more than a factor of about 100 over the intrinsic value. The typical boosting for blazar jets is expected on the level of about 10 or less (Lister et al., 2016). However, *Fermi* gamma-ray and TeV Cherenkov telescope results introduce significant complications — the “Doppler factor crisis.” Compton models that explain these high energy parts of the spectrum including the very short timescale TeV flares (e.g., Aharonian et al., 2007; Albert et al., 2007), require much larger Doppler factors than found from VLBI kinematics, and would imply observed radio core brightness temperatures higher than 10^{14} K.

The highest brightness temperature that can be measured by a radio interferometer does not depend on wavelength, but only on the physical baseline length and the accuracy of the fringe visibility measurement (see, e.g., Kovalev et al., 2005). Thus, going to shorter wavelengths does not help in measuring higher brightness temperatures. The highest brightness temperatures measured for AGN from the ground are of the order of 10^{13} K (e.g., Kovalev et al., 2005; Lisakov et al., 2017). This finding is consistent with the earlier VLBI observations from space conducted during the TDRSS experiments (Levy et al., 1989; Linfield et al., 1989, 1990) and in the framework of the VLBI Space Observatory Programme (VSOP, Frey et al., 2000; Horiuchi et al., 2004; Dodson et al., 2008). These observations probed baselines of up to 2.4 times the Earth diameter, but had a lower interferometric sensitivity compared to the more recent ground-based observations. Further increasing the baseline length is the only practical way to measure much higher brightness temperatures, and hence, to address the Compton Catastrophe issue. *RadioAstron* provides baselines up to 28 Earth diameters, allowing measurements of brightness temperature up to 10^{15} – 10^{16} K. This capability offers an unprecedented opportunity to place stringent observational constraints on the physics of the most energetic relativistic outflows. We underline that prior to the *RadioAstron* launch it was unknown if there were AGN compact and bright enough to be detected by a space VLBI system at baselines many times longer than the Earth diameter. An indirect evidence that AGN contain regions of an angular diameter in the range of 10–50 μas was provided by IDV measurements (e.g., Lovell et al., 2008).

RadioAstron results on selected individual sources were presented earlier by Kovalev et al. (2016); Edwards et al. (2017); Pilipenko et al. (2018); Kutkin et al. (2018) with an emphasis on the AGN brightness issue. In this paper we discuss *RadioAstron* detection results for a complete VLBI-flux-density limited sample of bright AGN jets.

2. Source sample and space VLBI observations

The *RadioAstron* AGN survey targets include the complete sample of 163 sources that have 8 GHz correlated flux densities at the ground baselines longer than $200 \text{ M}\lambda$ of $S_c > 600 \text{ mJy}$ as reported in the Radio Fundamental Catalog in 2012, at the time of the sample compilation². The large sample

²<http://astrogeo.org/rfc/>

size is essential for modeling the complex selection biases associated with relativistic beaming (e.g., Lister, 2003). Fig. 1 presents the redshift distribution of these AGN. The list of targets is augmented by AGN with jets showing the fastest speed (Lister et al., 2016), strong scintillators selected from intraday variability (IDV) surveys (e.g., Lovell et al., 2008), high redshift AGN, nearby AGN, and broad absorption line quasars. Here we discuss only the results related to the VLBI-flux-density limited sample.

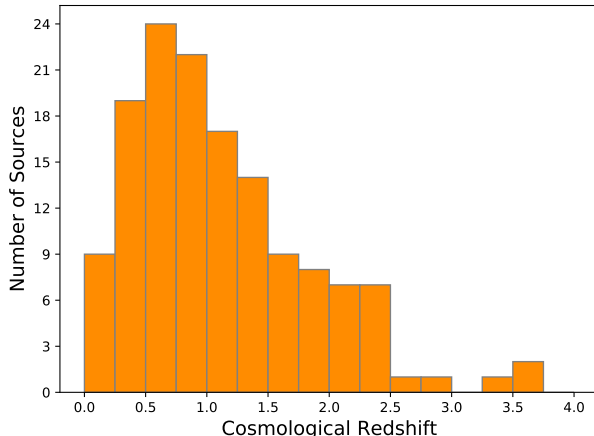


Figure 1: Redshift distribution of the complete VLBI-flux-density limited sample of 163 compact extragalactic radio sources.

An overview of the *RadioAstron* mission and the Spektr-R 10-m Space Radio Telescope (SRT) including its calibration is presented by Kardashev et al. (2013) and Kovalev et al. (2014). The AGN Survey observations were performed independently at three observing bands: 1.3 cm (K), 6 cm (C), and 18 cm (L). Terrestrially, the survey was supported by the following radio telescopes which have produced fringe detections with the SRT: Arecibo 305 m, phased Australia Telescope Compact Array (ATCA), Badary 32 m, Ceduna 30 m, Effelsberg 100 m, Evpatoria 70 m, Green Bank Telescope 100 m, Hartbeesthoek 26 m, Hobart 26 m, Irbene 32 m, Jodrell Bank 76 m, Kalyazin 64 m, Medicina 32 m, Mopra 22 m, Noto 32 m, Parkes 64 m, Robledo 70 m, Sheshan 25 m, Svetloe 32 m, Tianma 65 m, Torun 32 m, Usuda 64 m, phased Karl G. Jansky Very Large Array, phased Westerbork Synthesis Radio Telescope (WSRT), Yebes 40 m, and Zelenchukskaya 32 m. The AGN survey was also supported by long-term monitoring of the broad-band total flux density at RATAN-600 (1.4-31 cm) and OVRO (2 cm) radio telescopes as

well as intra-day variability measurements by Effelsberg (Liu et al., 2018), ATCA, WSRT, and Urumqi. The SRT recording rate was 128 Mbps with 1-bit sampling while ground telescopes utilized the 2-bit sampling with the total rate of 256 Mbps. The telescopes were recording 2×16 MHz channels per polarization.

RadioAstron detection sensitivity depends on the sensitivity of ground telescopes as well as coherence time for which we can integrate the data without significant losses. Accordingly, typical integration time at 18 and 6 cm was chosen to be up to 20 min while for 1.3 cm we have used 10 min long scans. Resulting detection sensitivity at the level of about 7σ with the largest ground telescopes was up to 6 mJy at 18 and 6 cm and 60 mJy at 1.3 cm.

The survey observations began within the *RadioAstron* Early Science Program and have continued as one of the Key Science Programs, spanning the years May 2012 – June 2016, inclusive. Each single-source space VLBI observation lasted for 40-60 minutes and was split into scans that are 10-20 minutes long being supported on the ground typically by several telescopes per frequency band. As the VLBI data collected by the SRT have to be downlinked to the ground in real time, a tracking station should be visible to the satellite’s steerable high-gain antenna during the observations. This, together with the SRT Sun-avoidance angles and the ground telescopes’ source visibility and scheduling constraints determine the planning of the survey observations. We used the **FakeRaT** software (Zhuravlev, 2015) based on the **FakeSat** code (Murphy, 1991; Murphy et al., 1994; Smith et al., 2000) to model the SRT-related constraints and **SCHED**³ to compute source visibility and generate **vex** control files for the ground telescopes. The Pushchino tracking station was utilized from the very beginning of the survey (Kardashev et al., 2013), while the Green Bank tracking station (Ford et al., 2014) joined the mission in August 2013. The *RadioAstron* VLBI experiments had to be separated by typically three-hour-long gaps to allow for the high-gain antenna drive to cool. Given the above constraints, an effort was made to observe each source multiple times to cover the full range of accessible space-ground baselines. The fast-evolving *RadioAstron* orbit provided a different range of baselines and baseline position angles for a given source over the years during which the survey was conducted. About 10% of the complete

³<http://www.aoc.nrao.edu/software/sched/>

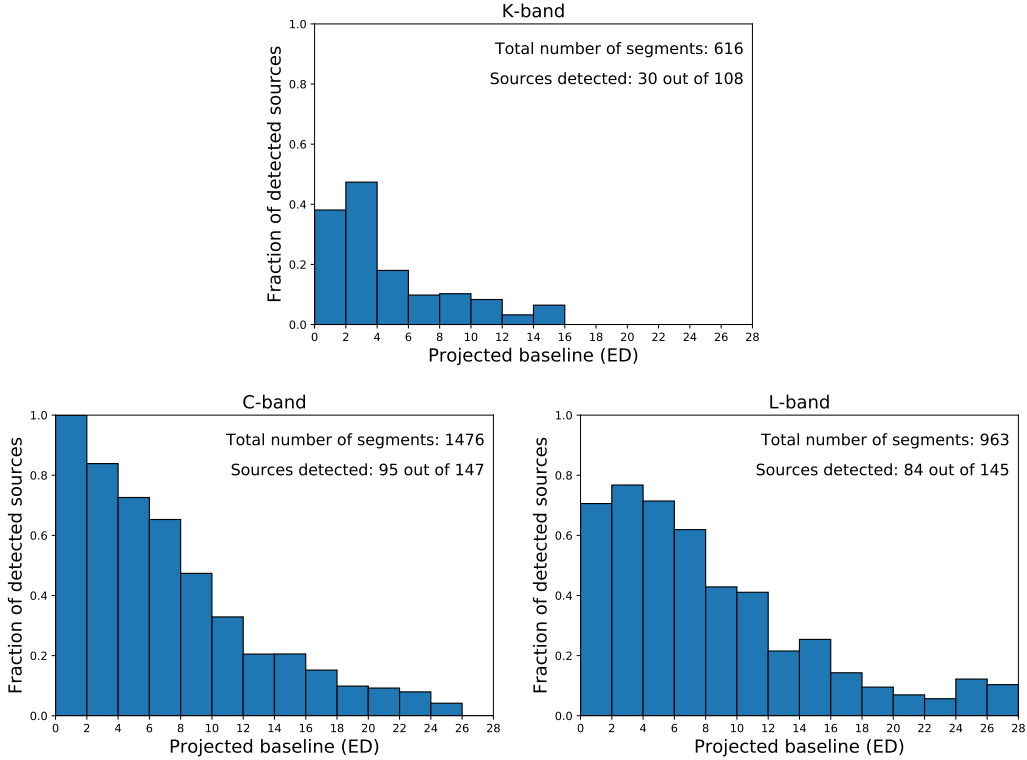


Figure 2: Fraction of detected sources versus projected ground-space VLBI baselines (in units of Earth diameters, ED) for 1.3 (K-band), 6 (C-band), and 18 cm (L-band) observations.

sample had not been observed by June 2016. These are the low-declination targets, which are more difficult to schedule due to the limited availability of telescopes in the Southern Hemisphere and stronger visibility restrictions of the SRT due to the absence of a tracking station in the South.

The survey focused on total intensity measurements. To increase the outcome of the observations, the following observing scheme was chosen. The SRT observed in a single-polarization dual-band mode. Typically, it was a combination of either L- and C-bands or C- and K-bands. An important advantage of this observing mode is the possibility of using the fringe detection from the lower frequency to check, or correct for, the Spektr-R orbit reconstruction uncertainty resulting in a large residual delay and its first and second derivatives for the higher frequency correlation and fringe search.

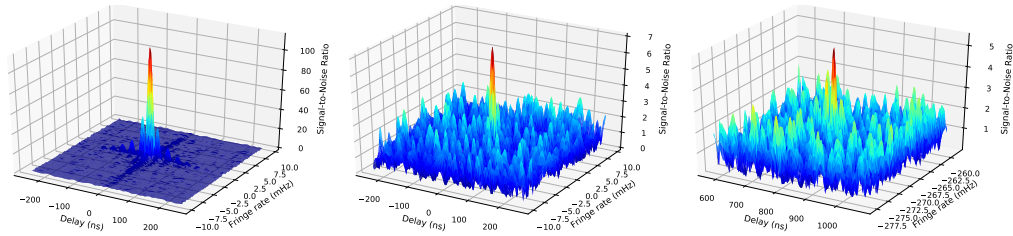


Figure 3: Examples of *RadioAstron* interferometric fringes, C-band observations of 0716+714. *Left panel*: Detection with $\text{PFD} < 10^{-100}$ at projected baseline 7.0 ED, SRT–Effelsberg, $\text{SNR}=138$; *middle panel*: detection with $\text{PFD} = 10^{-8}$ at projected baseline 21.9 ED, SRT–Effelsberg, $\text{SNR}=7.3$; *Right panel*: non-detection with $\text{PFD} = 0.07$ at projected baseline 22.0 ED, SRT–Noto, $\text{SNR}=5.3$

3. Space VLBI data analysis and detection results

The data were correlated by the Astro Space Center *RadioAstron* correlator in Moscow (Likhachev et al., 2017) and post-processed with the PIMA⁴ software (Petrov et al., 2011). The distribution of the fraction of detected sources versus projected *RadioAstron* baseline is presented in Fig. 2 for the three observing bands separately. A detection is considered significant if the probability of a false detection (PFD) is less than 0.01%. To determine the correspondence between the derived signal-to-noise ratio (SNR) and PFD for every observing scan we utilize the approach suggested by Petrov et al. (2011). We perform fringe fitting of AGN survey data and calculate an SNR statistic based on that (see examples in Fig. 3). The low-SNR part of this distribution represents non-detected sources, and therefore fitting to this part of the distribution with a theoretical function allows us to relate observed SNR to probability of false detection (Fig. 4). Note that the Figure presents the low-SNR part of the full set of SNR values only. We determine the parameters of this probability density distribution for the used sets of the following parameters: the number of spectral channels in a 16-MHz frequency channel, correlator integration time, and scan lengths (i.e. fringe search interval). From these parameters we calculate the PFD value corresponding to a given value of the SNR for each observing scan. An example of the empirical SNR distribution and the theoretical probability density distribution fit is shown in Fig. 4. *RadioAstron* has delivered detections in just over one third of the

⁴<http://astrogeo.org/pima/>

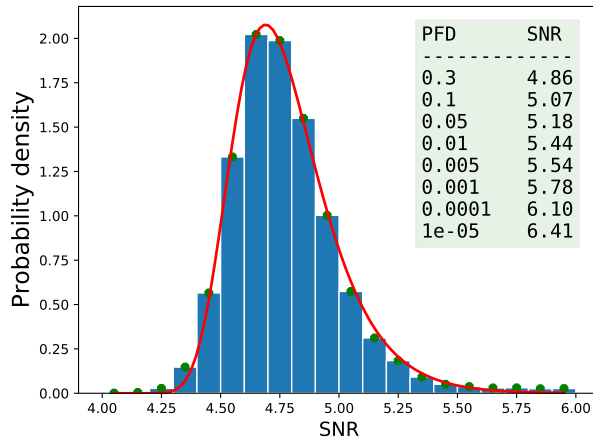


Figure 4: Low SNR part of the empirical distribution for the fringe SNR from the results of fringe fitting *RadioAstron* AGN Survey data. This particular distribution is obtained from 6 cm data correlated with the following parameters: 64 spectral channels per 16-MHz wide frequency channel, correlator integration time 0.5 s, and 10 min fringe search interval. The red curve is the theoretical distribution (Thompson et al., 2017) fitted to the low-SNR peak (the “no signal” case). The inset presents the correspondence between PFD and SNR for the given set of data parameters.

observing segments.

The survey observations were scheduled at a low priority level for short projected spacings in order to allow AGN imaging, as well as pulsar, maser, and gravitational redshift observations to reach their goals. As a result, the apparent drop in the detection fraction at 0 to 2 Earth Diameters (ED) can be observed in the K- and L-band histograms. Moreover, the ground support of those survey observations was poorer than average. This scheduling issue explains the apparent drop of the detection fraction at short baselines, which should be treated as an observational bias. The stronger statistics for the C-band observations results in a better, unbiased, first bin (Fig. 2).

About two thirds of the observed complete sample are detected on space VLBI baselines. This means that many AGN jets, most probably their cores (Kovalev et al., 2005), contain extremely compact regions of very bright synchrotron emission. The AGN which are detected at extreme projected spacing about or longer than 25 ED at L-band include 0048–097, 0106+013, 0119+115, 0235+164, 0716+714, 1253–055 and at C-band 0235+164, 1124–186. At K-band, detections at baseline projections about or longer than 15 ED or 14 $G\lambda$ are found from 0235+164, 0716+714, 0851+202. Many AGN de-

tected by *RadioAstron* are found to show brightness temperature values significantly in excess of the Compton Catastrophe limit and most of them are far above the equipartition value (Kellermann and Pauliny-Toth, 1969; Readhead, 1994).

It is of interest to note that the fractional detection histograms look similar to the median normalized projected fringe plots generated by the 6 cm VSOP (Horiuchi et al., 2004) and 2 cm VLBA (Kovalev et al., 2005) surveys. This basically reflects the core-jet structure of the observed targets but at the smaller scales probed. To first order, the difference between the detection histograms can be attributed to the different sensitivities. While the C-band and L-band observations have a comparable level of sensitivities, the K-band data are significantly less sensitive due to the following three reasons: the efficiencies of both ground and space telescopes are lower; their system temperatures are higher; and the coherence time at 1.3 cm is significantly shorter than at 6 and 18 cm due to the Earth’s troposphere.

We note a possible excess of fractional detections at the longest *RadioAstron* projected baselines at 18 cm in comparison to the 6 cm results of about the same sensitivity. This can be an indication of the scattering sub-structure originally discovered in *RadioAstron* pulsar observations (Gwinn et al., 2016; Popov et al., 2017) and later confirmed by the ground-based observations of Sgr A* (Gwinn et al., 2014; Johnson et al., 2018). See also the analyses of *RadioAstron* data for the quasars 3C 273 (Johnson et al., 2016) and B 0529+483 (Pilipenko et al., 2018).

These results also indicate that interstellar scattering only weakly affects the *RadioAstron* 6 cm results and is completely absent in 1.3 cm data, for the typical mid-Galactic latitude sight-lines probed by the survey, following estimations by Johnson and Gwinn (2015). Full results and analysis of the *RadioAstron* AGN survey data, as well as the methodology of *RadioAstron* observations, are currently being finalized in a number of papers.

4. Summary

In this paper we have presented the results of detection statistics for a complete sample of 163 AGN jets from 18, 6, and 1.3 cm observations by the ground-space interferometer *RadioAstron*. Two thirds of the targets have delivered significant interferometric fringes at space VLBI baselines indicating the presence of ultra-compact and bright structures within cores in many

of them. An excess of 18 cm detections at the longest *RadioAstron* baselines is attributed to the scattering sub-structure effect.

Acknowledgements

We thank Ken Kellermann, Chris Salter, Kristen Jones as well as anonymous referees for useful comments on the manuscript. The *RadioAstron* project is led by the Astro Space Center of the Lebedev Physical Institute of the Russian Academy of Sciences and the Lavochkin Scientific and Production Association under a contract with the State Space Corporation ROSCOSMOS, in collaboration with partner organizations in Russia and other countries. The results are partly based on observations performed with radio telescopes of IAA RAS, the 100-m telescope of the MPIfR (Max-Planck-Institute for Radio Astronomy) at Effelsberg, the Medicina and Noto telescopes operated by INAF – Istituto di Radioastronomia, the Sheshan and Tianma telescopes operated by Shanghai Astronomical Observatory of Chinese Academy of Sciences, the DSS-63 antenna at the Madrid Deep Space Communication Complex under the Host Country Radio Astronomy program. The paper has used the Evpatoria RT-70 radio telescope (Ukraine) observations carried out by the Institute of Radio Astronomy of the National Academy of Sciences of Ukraine under a contract with the State Space Agency of Ukraine and by the National Space Facilities Control and Test Center with technical support by Astro Space Center of Lebedev Physical Institute, Russian Academy of Sciences. This work is based in part on observations carried out using the 32-meter radio telescope operated by Torun Centre for Astronomy of Nicolaus Copernicus University in Torun (Poland) and supported by the Polish Ministry of Science and Higher Education SpUB grant. The Hartebeesthoek telescope is a facility of the National Research Foundation of South Africa. The Arecibo Observatory is operated by SRI International under a cooperative agreement with the National Science Foundation (AST-1100968), and in alliance with Ana G. Mendez-Universidad Metropolitana, and the Universities Space Research Association. The Green Bank Observatory is a facility of the National Science Foundation operated under cooperative agreement by Associated Universities, Inc. The Long Baseline Array is part of the Australia Telescope National Facility which is funded by the Australian Government for operation as a National Facility managed by CSIRO. Results of optical positioning measurements of the Spektr-R spacecraft by the global MASTER Robotic Net (Lipunov et al., 2010), ISON

collaboration, and Kourovka observatory were used for spacecraft orbit determination in addition to mission facilities.

References

- Aharonian, F., Akhperjanian, A.G., Bazer-Bachi, A.R., et al., 2007. An Exceptional Very High Energy Gamma-Ray Flare of PKS 2155-304. *ApJL* 664, L71–L74. doi:10.1086/520635, arXiv:0706.0797.
- Albert, J., Aliu, E., Anderhub, H., et al., 2007. Variable Very High Energy γ -Ray Emission from Markarian 501. *ApJ* 669, 862–883. doi:10.1086/521382, arXiv:astro-ph/0702008.
- Cohen, M.H., Lister, M.L., Homan, D.C., et al., 2007. Relativistic Beaming and the Intrinsic Properties of Extragalactic Radio Jets. *ApJ* 658, 232–244. doi:10.1086/511063, arXiv:astro-ph/0611642.
- Dodson, R., Fomalont, E.B., Wiik, K., et al., 2008. The VSOP 5 GHz Active Galactic Nucleus Survey. V. Imaging Results for the Remaining 140 Sources. *ApJS* 175, 314–355. doi:10.1086/525025, arXiv:0710.5707.
- Edwards, P.G., Kovalev, Y.Y., Ojha, R., et al., 2017. PKS 1954-388: RadioAstron Detection on 80,000 km Baselines and Multiwavelength Observations. *PASA* 34, e021. doi:10.1017/pasa.2017.16, arXiv:1705.02067.
- Ford, H.A., Anderson, R., Belousov, K., et al., 2014. The RadioAstron Green Bank Earth Station, in: *Proceedings of the SPIE. Ground-based and Airborne Telescopes V*, p. 91450B. doi:10.1117/12.2056761.
- Frey, S., Gurvits, L.I., Altschuler, D.R., et al., 2000. Dual-Frequency VSOP Observations of AO 0235+164. *PASJ* 52, 975–982. arXiv:arXiv:astro-ph/0007347.
- Gwinn, C.R., Kovalev, Y.Y., Johnson, M.D., Soglasnov, V.A., 2014. Discovery of Substructure in the Scatter-broadened Image of Sgr A*. *ApJL* 794, L14. doi:10.1088/2041-8205/794/1/L14, arXiv:1409.0530.
- Gwinn, C.R., Popov, M.V., Bartel, N., et al., 2016. PSR B0329+54: Statistics of Substructure Discovered within the Scattering Disk on RadioAstron Baselines of up to 235,000 km. *ApJ* 822, 96. doi:10.3847/0004-637X/822/2/96, arXiv:1501.04449.

- Horiuchi, S., Fomalont, E.B., Taylor, W.K., et al., 2004. The VSOP 5 GHz Active Galactic Nucleus Survey. IV. The Angular Size/Brightness Temperature Distribution. *ApJ* 616, 110–122. doi:10.1086/424811, arXiv:arXiv:astro-ph/0407069.
- Johnson, M.D., Gwinn, C.R., 2015. Theory and Simulations of Refractive Substructure in Resolved Scatter-broadened Images. *ApJ* 805, 180. doi:10.1088/0004-637X/805/2/180, arXiv:1502.05722.
- Johnson, M.D., Kovalev, Y.Y., Gwinn, C.R., et al., 2016. Extreme Brightness Temperatures and Refractive Substructure in 3C273 with RadioAstron. *ApJL* 820, L10. doi:10.3847/2041-8205/820/1/L10, arXiv:1601.05810.
- Johnson, M.D., Narayan, R., Psaltis, D., et al., 2018. The Scattering and Intrinsic Structure of Sagittarius A* at Radio Wavelengths. *ApJ* 865, 104. doi:10.3847/1538-4357/aadcff, arXiv:1808.08966.
- Kardashev, N.S., Khartov, V.V., Abramov, V.V., et al., 2013. “RadioAstron”—A telescope with a size of 300 000 km: Main parameters and first observational results. *Astronomy Reports* 57, 153–194. doi:10.1134/S1063772913030025, arXiv:1303.5013.
- Kellermann, K.I., Pauliny-Toth, I.I.K., 1969. The Spectra of Opaque Radio Sources. *ApJL* 155, L71–L78. doi:10.1086/180305.
- Kovalev, Y.A., Vasil’kov, V.I., Popov, M.V., et al., 2014. The RadioAstron project: Measurements and analysis of basic parameters of space telescope in flight in 2011-2013. *Cosmic Research* 52, 393–402. doi:10.1134/S0010952514050074.
- Kovalev, Y.Y., Kardashev, N.S., Kellermann, K.I., et al., 2016. RadioAstron Observations of the Quasar 3C273: A Challenge to the Brightness Temperature Limit. *ApJL* 820, L9. doi:10.3847/2041-8205/820/1/L9, arXiv:1601.05806.
- Kovalev, Y.Y., Kellermann, K.I., Lister, M.L., et al., 2005. Sub-Milliarcsecond Imaging of Quasars and Active Galactic Nuclei. IV. Fine-Scale Structure. *AJ* 130, 2473–2505. doi:10.1086/497430, arXiv:arXiv:astro-ph/0505536.

- Kutkin, A.M., Pashchenko, I.N., Lisakov, M.M., et al., 2018. The extreme blazar AO 0235+164 as seen by extensive ground and space radio observations. *MNRAS* 475, 4994–5009. doi:10.1093/mnras/sty144, arXiv:1801.04892.
- Levy, G.S., Linfield, R.P., Edwards, C.D., et al., 1989. VLBI using a telescope in Earth orbit. I - The observations. *ApJ* 336, 1098–1104. doi:10.1086/167080.
- Likhachev, S.F., Kostenko, V.I., Girin, I.A., et al., 2017. Software Correlator for Radioastron Mission. *Journal of Astronomical Instrumentation* 6, 1750004–131. doi:10.1142/S2251171717500040, arXiv:1706.06320.
- Linfield, R.P., Levy, G.S., Edwards, C.D., et al., 1990. 15 GHz space VLBI observations using an antenna on a TDRSS satellite. *ApJ* 358, 350–358. doi:10.1086/168992.
- Linfield, R.P., Levy, G.S., Ulvestad, J.S., et al., 1989. VLBI using a telescope in Earth orbit. II - Brightness temperatures exceeding the inverse Compton limit. *ApJ* 336, 1105–1112. doi:10.1086/167081.
- Lipunov, V., Kornilov, V., Gorbovskoy, E., et al., 2010. Master Robotic Net. *Advances in Astronomy* 2010, ID 349171 (6 pages). doi:10.1155/2010/349171, arXiv:0907.0827.
- Lisakov, M.M., Kovalev, Y.Y., Savolainen, T., Hovatta, T., Kutkin, A.M., 2017. A connection between γ -ray and parsec-scale radio flares in the blazar 3C 273. *MNRAS* 468, 4478–4493. doi:10.1093/mnras/stx710, arXiv:1703.07976.
- Lister, M.L., 2003. Gigahertz Peaked Spectrum Radio Sources, in: *ASP Conf. Ser. 300, Radio Astronomy at the Fringe*, San Francisco: ASP. pp. 71–79.
- Lister, M.L., Aller, M.F., Aller, H.D., et al., 2016. MOJAVE: XIII. Parsec-scale AGN Jet Kinematics Analysis Based on 19 years of VLBA Observations at 15 GHz. *AJ* 152, 12. doi:10.3847/0004-6256/152/1/12, arXiv:1603.03882.

- Liu, J., Bignall, H., Krichbaum, T., et al., 2018. Effelsberg Monitoring of a Sample of RadioAstron Blazars: Analysis of Intra-Day Variability. *Galaxies* 6, 49. doi:10.3390/galaxies6020049, arXiv:1804.09289.
- Lovell, J.E.J., Rickett, B.J., Macquart, J.P., et al., 2008. The Micro-Arcsecond Scintillation-Induced Variability (MASIV) Survey. II. The First Four Epochs. *ApJ* 689, 108–126. doi:10.1086/592485, arXiv:0808.1140.
- Murphy, D.W., 1991. Simulations of space VLBI, in: Cornwell, T.J., Perley, R.A. (Eds.), *IAU Colloq. 131: Radio Interferometry. Theory, Techniques, and Applications*, ASP: San Francisco. pp. 107–111.
- Murphy, D.W., Yakimov, V., Kobayashi, H., Taylor, A.R., Fejes, I., 1994. Space VLBI Simulations, in: Sasao, T., Manabe, S., Kameya, O., Inoue, M. (Eds.), *VLBI Tecnology: Progress and Future Observational Possibilities*, Terra Scientific Publishing Company: Tokyo. pp. 34–38.
- Petrov, L., Kovalev, Y.Y., Fomalont, E.B., Gordon, D., 2011. The Very Long Baseline Array Galactic Plane Survey – VGaPS. *AJ* 142, 35. doi:10.1088/0004-6256/142/2/35, arXiv:1101.1460.
- Pilipenko, S.V., Kovalev, Y.Y., Andrianov, A.S., et al., 2018. The high brightness temperature of B0529+483 revealed by RadioAstron and implications for interstellar scattering. *MNRAS* 474, 3523–3534. doi:10.1093/mnras/stx2991, arXiv:1711.06713.
- Popov, M.V., Bartel, N., Gwinn, C.R., et al., 2017. PSR B0329+54: substructure in the scatter-broadened image discovered with RadioAstron on baselines up to 330 000 km. *MNRAS* 465, 978–985. doi:10.1093/mnras/stw2353, arXiv:1609.04008.
- Readhead, A.C.S., 1994. Equipartition brightness temperature and the inverse Compton catastrophe. *ApJ* 426, 51–59. doi:10.1086/174038.
- Shklovskii, I.S., 1964. Nature of Jets in Radio Galaxies. *Soviet Ast.* 7, 748–754.
- Smith, J.G., Meier, D.L., Murphy, D.W., et al., 2000. JPL Contribution to the VSOP Mission. *Advances in Space Research* 26, 637–640. doi:10.1016/S0273-1177(99)01206-5.

Thompson, A.R., Moran, J.M., Swenson, Jr., G.W., 2017. Interferometry and Synthesis in Radio Astronomy, 3rd Edition. doi:10.1007/978-3-319-44431-4.

Zhuravlev, V.I., 2015. Fakerat software in the international interferometric radioastron project with very long ground-space bases. Cosmic Research 53, 216–225. doi:10.1134/S0010952515030090, arXiv:1404.2430.